Numerical investigation of subcooled flow boiling in an inclined rectangular mini-channel at a low flow rate (EP)

(iD) **Yu-Jie Chen** (陈宇杰), (iD) **Ge-Ge Song** (宋阁阁), **Kong Ling** (凌空), **et al.**

COLLECTIONS

Paper published as part of the special topic on Multiphase flow in energy studies and applications: A special issue for MTCUE-2022

(EP) This paper was selected as an Editor's Pick

View Online   Export Citation   CrossMark

ARTICLES YOU MAY BE INTERESTED IN

Pore-scale study of mineral dissolution in heterogeneous structures and deep learning prediction of permeability
Physics of Fluids **34**, 116609 (2022); https://doi.org/10.1063/5.0123966

Simulation of liquid jet atomization and droplet breakup via a Volume-of-Fluid Lagrangian–Eulerian strategy
Physics of Fluids **34**, 113326 (2022); https://doi.org/10.1063/5.0122742

Unsteady flow and pressure pulsation characteristics in centrifugal pump based on dynamic mode decomposition method
Physics of Fluids **34**, 112014 (2022); https://doi.org/10.1063/5.0097223

Physics of Fluids

Special Topic: Paint and Coating Physics

Submit Today!

AIP Publishing

Numerical investigation of subcooled flow boiling in an inclined rectangular mini-channel at a low flow rate (EP)

Yu-Jie Chen (陈宇杰),[1,2] (iD) Ge-Ge Song (宋阁阁),[3] (iD) Kong Ling (凌空),[1] Bo Yu (宇波),[2] (iD) Dongliang Sun (孙东亮),[2] (iD) Wei Lu (路伟),[4] (iD) and Wen-Quan Tao (陶文铨)[1,a] (iD)

AFFILIATIONS

[1]Key Laboratory of Thermo-Fluid Science and Engineering, Ministry of Education, School of Energy and Power Engineering, Xi'an Jiaotong University, Shaanxi 710049, China
[2]School of Mechanical Engineering, Beijing Key Laboratory of Pipeline Critical Technology and Equipment for Deepwater Oil and Gas Development, Beijing Institute of Petrochemical Technology, Beijing 102617, China
[3]School of Chemical Engineering and Technology, Xi'an Jiaotong University, Shaanxi 710049, China
[4]State Key Laboratory of Alternate Electrical Power System with Renewable Energy Sources, North China Electric Power University, Beijing 102206, China

Note: This paper is part of the special topic, Multiphase flow in energy studies and applications: A special issue for MTCUE-2022.
[a]Author to whom correspondence should be addressed: wqtao@mail.xjtu.edu.cn

ABSTRACT

Under a low flow rate, gravity may become prominent for bubble behavior and heat transfer of flowing boiling because of the weakness of drag force from liquid, and its effect changes with the inclination angle of the mini-channel but without consensus. In this paper, based on a reasonable nucleus site density model and considering conjugate heat transfer, the coupled volume-of-fluid and level set method is adopted to study the subcooled flow boiling in an inclined three-dimensional rectangular mini-channel ($0°-180°$) with a characteristic size of 1.0 mm at a low flow rate of 88.8 kg m^{-2} s^{-1}. The inclination angle is found to have a slight effect on the flow boiling, which is different from the conclusion drawn based on the traditional-macro channel. A bubbly flow appears when a heat flux of 300 kW/m^2 is added. An unconventional impact force is proposed, which presses large bubbles to slip along the heating wall, with slight differences in the flow pattern under different inclination angles. When the inclination angle is close to $0°$, the upstream small/medium bubbles leave the heating wall under gravitational effects, which is conducive to heat transfer. As the inclination angle approaches $90°$, gravity pushes the large bubbles downstream to leave the channel, favoring the rewetting of the dry patches below. These two positive effects fail as the inclination angle approaches $180°$, leading to slightly worse overall heat exchange efficiency. However, the maximum differences in the average and local wall superheating of the mini-channel are only 8.4% and 22.5%, respectively, across the range of inclination angles because the flow pattern remains similar under the effect of the impact force. In addition, the effect of inclination angle on flow boiling becomes weaker with the increase in heat flux because of happening of slug flow.

Published under an exclusive license by AIP Publishing. https://doi.org/10.1063/5.0115599

I. INTRODUCTION

The trend for higher-frequency operations in electronic systems results in high thermal management requirements. Flow boiling is an efficient heat exchange technique, removing large amounts of heat through the disturbance and phase change generated by the formation and evolution of bubbles. Electronic equipment can be stored in a relatively safe and efficient operation range under flow-boiling heat transfer, which is widely used in other fields, such as nuclear energy, petrochemicals, and aerospace.[1,2] A critical factor affecting flow-boiling heat transfer is bubble dynamics, which is related to surface tension force, drag force, Marangoni force, gravity, shear lift force, etc.[3,4] For the pool boiling, under micro-gravity, the gravitational flow on the ground is changed into the surface-tension flow,[5] affecting the heat transfer performance. In addition, the buoyant force is inadequate to overcome wall adhesion in low gravity, and a central bubble appears and remains attached to the surface leading to low heat flux.[6]

Regarding flow boiling, flow instabilities under microgravity might happen easier,[7] and interfacial behavior and heat transfer mechanisms are different from those under Earth's gravity.[8] Therefore, gravity has significant effects on boiling heat transfer. The component of gravity normal or parallel to the heat exchange surface varies with the inclination angle, leading to the different impacts on the bubble and flow-boiling heat transfer under different application scenarios, especially at low flow rates because of the weak forced convection effect.

The critical heat flow (CHF) and the heat transfer coefficient (HTC) are the two main parameters concerned in experimental studies of the inclination angle effect on flow-boiling heat transfer at a low flow rate. Regarding the channel inclination effect on CHF, Zhang et al.[9] employed a rectangular channel with a cross section of $2.5 \times 5.0\,mm^2$ to investigate the effect of inclination angles from $0°$ to $360°$ on the critical heat flux of FC-72 using high-speed video and micrograph techniques. Under large flow velocities, the generation of a wavy vapor layer triggered the boiling crisis, regardless of the included angle between the gravitational force and the channel. In contrast, different mechanisms triggered the boiling crisis at low speeds under different inclination angles. Kharangate et al.[10] studied the CHF of FC-72 in a similar rectangular channel to that used by Zhang et al.[9] Their results showed that when the mass flow rate was low, gravity played a leading role in the vapor–liquid interface behavior, and the lowest (respectively, highest) CHF occurred under heating by the top wall (respectively, bottom wall). With an increase in the mass flow rate, the effect of the inclination angle on the CHF decreased and totally disappeared under very high mass flows. Gersey and Mudawar[11] adopted FC-72 to explore the CHF of flow boiling in a $5.0 \times 20.0\,mm^2$ channel and found that the CHF was independent of the inclination angle at flow velocities greater than 2 m/s. Based on a small channel with a characteristic cross section of $2.5 \times 5.0\,mm^2$, Zhang et al.[12,13] found that the CHF of saturated flow boiling changed with the pipe inclination angle at a flow rate of 0.2 m/s, and an increase in flow rate or subcooling inhibited the effect of the inclination angle on the CHF.

Regarding the channel inclination effect on the HTC of flow boiling, Piasecka et al.[14–16] adopted FC-72 as the working fluid in a narrow channel with dimensions of $1 \times 40\,mm^2$. Their results indicated that the channel inclination significantly affected the HTC at a flow rate of 0.211 m/s. The highest HTC occurred when the inclination angle was $90°$ for the saturated condition and $45°$ for the subcooled flow boiling. The worst heat transfer performance for both saturated and subcooled flow boiling was found to occur at an inclination angle of $180°$. Hu et al.[17] investigated the effect of inclination on the average HTC of flow boiling in a copper tube with a diameter of 4 mm. The maximum difference in the HTC among different inclination angles was only 10% in the flow velocity range of 0.167–0.287 m/s, which was within the experimental measurement error. Chen et al.[18] studied the effect of the inclination angle on flow-boiling heat transfer in a heat sink with a hydraulic diameter of 0.91 mm. The boiling curves of different inclined heat sink almost coincided in the low-flow-velocity range of 0.12–0.5 m/s, indicating that the influence of gravity on boiling heat transfer was greatly weakened in fine channels. Mei[19] explored the HTC of an inclined macro-channel with a characteristic size of $12.6 \times 12.6\,mm^2$. Under a low-flow-velocity range of 0.11–0.3 m/s, the HTC changed slightly over inclination angles of $45°–90°$, for which the magnitude of the HTC was larger than that within the range $15°–45°$. Furthermore, Mei et al.[20] found that the inclination of the heating surface affected

the HTC and CHF in the case of pool boiling. Abadi et al.[21] investigated the effect of horizontal and vertical tubes with a characteristic size of 3 mm on the HTC of flow boiling. At the same mass flow rate, the vertical flow transited into an annular flow earlier than the horizontal flow, and the vertical flow exhibited a higher HTC and lower pressure drop.

Most of the above experimental studies suggest that the inclination angle has significant impacts on the CHF or HTC at low flow rates (termed the supportive view),[9–16,20,21] but other few studies take an opposing view,[17,18] especially for channels with small characteristic sizes.[18] A hydraulic diameter of 3 mm is generally used to distinguish between macro- and mini-channels.[22] Under low flow rates, researchers with the supportive view have employed macro-channels,[9–16,20,21] whereas those with the opposing view have considered both macro-[17] and mini-channels.[18] When the channel geometry is reduced, the bubble detachment diameter is approximately equal to the channel characteristic size. This may prevent the bubble from detaching properly from the heating surface, so the effect of the inclination angle on the flow-boiling heat transfer at low flow rates in mini-channels may be different from that in macro-channels. However, there have been few related experimental studies. With the development of compact equipment, the heat dissipation space has been compressed, and the effects of inclination angle on flow-boiling heat transfer in mini-channels at low flow velocities require urgent investigation. However, experimental studies of flow boiling become more difficult as the channel size decreases.

Numerical simulations can obtain more information and separate the influence variables in the study of boiling,[23,24] making them an important supplement to experiments. Nie and Guan[25] adopted the lattice Boltzmann method (LBM) to investigate the effect of shear flow on boiling heat transfer under gravity, founding that the shear flow accelerated bubble departure for hydrophobic surfaces. However, the lattice Boltzmann method did not handle the situation with the real density ratio and viscosity ratio.[25–28] This deficiency can be eliminated by the computational fluid dynamics method (CFD). Li and Dhir[29] employed the level set (LS) method to study the effect of the inclination angle in a three-dimensional channel on the dynamic characteristics of a single bubble. Their results showed that the bubble detachment diameter increases with the inclination angle. Chen et al.[30] used the moving particle semi-implicit method to investigate the inclination angle effect on a single two-dimensional bubble and found that it affected the bubble detachment diameter and time. Vermaak et al.[31] adopted the volume-of-fluid (VOF) method to study the effect of the inclination angle on single bubble growth in two- and three-dimensional channels, and obtained similar conclusions to those of Chen et al.[30] Zhang et al.[32] explored the flow-boiling heat transfer of R32 in a two-dimensional inclined pipe with an inner diameter of 1 mm using the VOF method. The results indicated that, under mass flow rates of 100 and $300\,kg/(m^2\,s)$, the HTC clearly decreased with increasing inclination angle in the inlet section, while only slight changes occurred in the middle and outlet regions. Overall, the expectant complementation between experiment and simulation studies has not been achieved. There have been insufficient numerical simulations of the flow-boiling heat transfer in inclined channels, and most previous studies focus on a single bubble and are far from the actual flow boiling, leading to a gap in revealing the inclination angle effect on flow-boiling heat transfer in mini-channels at low flow rates.
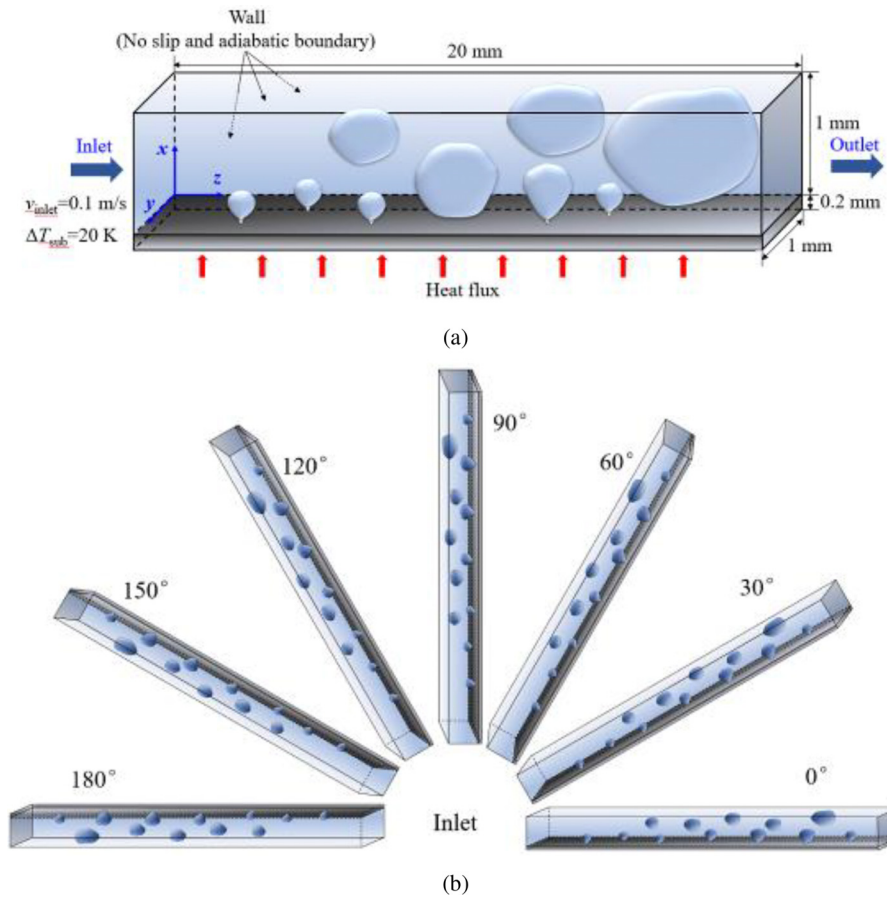
(a)

(b)

In this paper, based on a reasonable nucleus site density model and considering conjugate heat transfer, the subcooled flow-boiling heat transfer in three-dimensional inclined rectangular mini-channels at low flow rates is numerically studied using a combined VOF and LS method (VOSET). In-depth analyses of the flow patterns and heat exchange for inclination angles of 0°–180° illustrate the relationship between inclination angle and flow boiling at a low flow rate, and provide support for the existing flow-boiling heat transfer theory and enhancement technology in mini-channels.

II. PROBLEM DESCRIPTION

This paper investigates the subcooled flow-boiling heat transfer in an inclined mini-channel at a low flow rate. As displayed in Fig. 1(a), the research object is a three-dimensional rectangular mini-channel with a size of $1.0\ (x) \times 1.0\ (y) \times 20.0\ mm^3\ (z)$. A silicon plate with a size of $1.0\ (x) \times 0.2\ (y) \times 20.0\ mm^3\ (z)$ acts as the heating wall, and a constant heat flux of $300\ kW/m^2$ is added to its outside. The contact angle of the silicon plate is $50°$, and the other three sides of the channel are no-slip walls. The fluid with a subcooling of 20 K flows from the inlet at 0.1 m/s and exchanges heat with the wall through conjugate heat transfer. The system pressure is 1.0 MPa, the corresponding fluid saturation temperature is 453 K, the latent heat is 2.02×10^6 J/kg, and the surface tension of the vapor–liquid interface is 0.042 N/m. The other physical properties are listed in

Table I. The inclination angle ranges from 0 to 180°, as shown in Fig. 1(b). When the inclination angle is 0°–90°, the component of gravity in the direction perpendicular to the wall points to the wall, which promotes the bubble detachment. The gravity component direction and effect are reversed when the inclination angle is from 90° to 180°.

III. NUMERICAL MODELS

A. Governing equations

In this study, a complex and comprehensive numerical method is adopted to predict flow boiling in the mini-channel. The solid wall is subject to the transient heat conduction equation shown in Eq. (1). Solving the fluid region is very complex as it includes numerical descriptions of the flow, convective and conjugated heat transfer, phase transition, vapor–liquid interface reconstruction, and bubble

TABLE I. Physical properties of study media.

	Density (kg/m^3)	Viscosity (Pa s)	Thermal conductivity (W/(m K))	Heat capacity (J/(kg K))
Wall	2330.0	$\cdots$	148.0	766.0
Liquid	888.10	1.51×10^{-4}	0.674	4400.0
Vapor	5.14	1.50×10^{-5}	0.036	2712.0

nucleation, and their solving methods are introduced successively next. The flow is described by the continuity and momentum equations presented in Eqs. (2) and (3). The vapor–liquid interface temperature acts as a constant-temperature boundary with a value set to the saturation temperature, and heat transfer inside the liquid and vapor regions is solved by the energy equation, as shown in Eqs. (4) and (5). The phase transition only happens at the vapor–liquid interface and is calculated by the Rankine–Hugoniot jump condition without any empirical parameters,[33,34] as described by Eqs. (6) and (7). The vapor–liquid interface is captured by the accurate VOSET method,[35,36] which combines the advantages of the VOF and LS methods with a relatively low computational cost,

$$\frac{\partial(\rho_s c_s T)}{\partial t} = \nabla \cdot (\lambda_s \nabla T), \tag{1}$$

$$\nabla \cdot \mathbf{u} = \left(\frac{1}{\rho_v} - \frac{1}{\rho_l}\right)\dot{m}, \tag{2}$$

$$\frac{\partial(\rho\mathbf{u})}{\partial t} + \nabla \cdot (\rho\mathbf{u}\mathbf{u}) = -\nabla p + \nabla \cdot \left[(\eta + \eta_t)(\nabla\mathbf{u} + \nabla\mathbf{u}^T)\right] + \mathbf{f} + \rho\mathbf{g}, \tag{3}$$

$$\frac{\partial(\rho_l c_{p,l} T)}{\partial t} + \nabla \cdot (\rho c_{p,l} \mathbf{u} T) = \nabla \cdot (\lambda_l \nabla T), \tag{4}$$

$$\frac{\partial(\rho_v c_{p,v} T)}{\partial t} + \nabla \cdot (\rho c_{p,v} \mathbf{u} T) = \nabla \cdot (\lambda_v \nabla T), \tag{5}$$

$$\int_V \dot{m}\,dV = \frac{1}{h}\int_A \dot{q}\,dA, \tag{6}$$

$$\dot{q} = \lambda_v \frac{\partial T}{\partial n}\bigg|_v - \lambda_l \frac{\partial T}{\partial n}\bigg|_l, \tag{7}$$

where ρ is the density, kg/m^3; c is the heat capacity, J/(kg K); λ is the thermal conductivity, W/(m K); $\dot{m}$ is the phase change rate, kg/(m^3 s); η is the dynamic viscosity, Pa s; η_t is the turbulent viscosity calculated by the Smagorinsky model,[37] Pa s; $\mathbf{f}$ is the surface tension calculated by the CSF model,[38] N/m^3; $\mathbf{g}$ is gravity, m/s^2; h is the latent heat of water; $\dot{q}$ is the heat flux caused by phase transition;[33] and the indexes s, l, and v represent solid, liquid, and vapor, respectively.

The phase transition model used in this study cannot describe the bubble nucleation process at the nanoscale, and how to reasonably determine the nucleation position and condition is challenging for direct numerical simulation. In this study, considering the studied high-pressure condition (1 MPa), an extra nucleus site density model with a wide applied range proposed by Li et al.[39] is used to describe heterogeneous nucleation, as shown in Eqs. (8)–(12). It is worth emphasizing that combining the nucleus site density model obtained by the experiment with the phase transition model can achieve a more reasonable simulation of flow boiling because the nucleation described by the existing macro method is unphysical and unreasonable,

$$N_w = N_0(1 - \cos\theta)\exp\left[f(P)\right]\Delta T_{sup}^{A\Delta T_{sup}+B}, \tag{8}$$

$$f(P) = 26.006 - 3.678\exp(-2P) - 21.907\exp\left(-\frac{P}{24.065}\right), \tag{9}$$

$$A = -0.0002P^2 + 0.0108P + 0.0119, \tag{10}$$

$$B = 0.122P + 1.988, \tag{11}$$

$$1 - \cos\theta = (1 - \cos\theta_0)\left(\frac{T_c - T_{sat}}{T_c - T_0}\right)^\gamma, \tag{12}$$

where $N_0 = 1000$ site/m^2, $\theta_0 = 41.37°$, $T_c = 374\,°C$, $T_0 = 25\,°C$, $\gamma = 0.719$ by default.[40]

In this study, the wall superheating decides the nucleus site density because the contact angle and pressure are fixed. The implementation procedures of the nucleus site density model are introduced as follows: First, calculate the nucleus site number every $\Delta T = 0.1$ K; Then, record the nucleus site number N_0 and N_1 for ΔT_{sup} and $\Delta T_{sup} + \Delta T$. Here, $N_1 - N_0$ is the number of nucleus site with the activated superheating of over $\Delta T_{sup} + \Delta T$; Finally, put these nucleus sites randomly on the heating wall, and store the corresponding position and activated superheating. As shown in Fig. 2, the activated wall superheating of the black, red, and blue sites are over 3.0, 3.1, and 3.2 K, respectively. It is noteworthy that Fig. 2 is just a sketch, and thousands of nucleus sites are set on the heating wall with the corresponding activated conditions in this study. Once a nucleus site is activated, an artificial bubble nucleus with a radius of one grid length is put there. In addition, the nucleus site density model will fail if the Dirichlet boundary condition is applied for the heating wall without thickness. Therefore, in this study, the conjugate heat transfer between silicon plate and fluid is considered based on the temperature and heat flux continuity principles, as described in Eqs. (13) and (14) and Fig. 3,

$$T_n = T_{n,f} = T_{n,s}, \tag{13}$$

$$q_n = \frac{T_N - T_n}{\frac{(\delta y)_n^+}{\lambda_f}} = \frac{T_n - T_S}{\frac{(\delta y)_n^-}{\lambda_s}} = \frac{T_N - T_S}{\frac{(\delta y)_n^+ + (\delta y)_n^-}{\lambda_{eff}}}, \tag{14}$$

where λ_{eff} is the effective thermal conductivity at the solid–fluid interface, W m^{-1} K^{-1}; q_n represents heat flux through the solid–fluid interface, W/m^2.

The discretization schemes for the transient term, convection term, and diffusion term of momentum and energy equations are
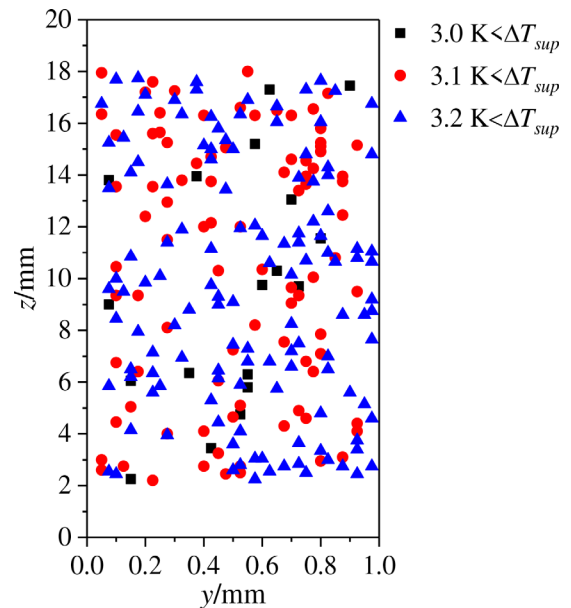

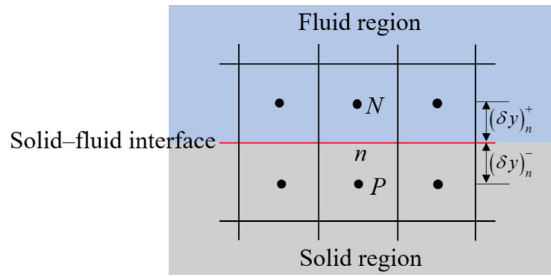FIG. 2. Sketch of nucleus site and activated condition.

FIG. 3. Sketch of nodes near the solid–fluid interface.

first-order forward difference, MUSCL (monotonic upwind scheme for conservation laws), and central difference schemes, respectively. In addition, several limitations in the time step are made to improve numerical stability.[41] Generally, the time step is less than 1.0×10^{-6} s during the simulation,

$$\Delta t \leq 0.8 \frac{\rho_v \Delta x^2}{6\eta_v}, \quad (15)$$

$$\Delta t \leq 0.8 \frac{\rho_l \Delta x^2}{6\eta_l}, \quad (16)$$

$$\Delta t \leq 0.5 \sqrt{\frac{(\rho_l + \rho_v)\Delta x^3}{\pi\sigma}}, \quad (17)$$

$$\Delta t \leq 0.1 \frac{\Delta x}{|u|_{max}}, \quad (18)$$

where Δx is grid step; σ is liquid–vapor surface tension coefficient; and $|u|_{max}$ is the absolute value of maximum velocity.

As shown in Fig. 1(a), the boundary conditions are set as follows: constant velocity and temperature boundaries are adopted at the inlet; the outlet is a free outflow boundary; the outside of the heating wall is a constant heat flux boundary; the other walls are adiabatic and no-slip boundaries.

Based on the above governing equations and boundary conditions, the pressure, velocity, and temperature fields are solved successively. The projection algorithm is adopted to obtain coupled solutions of the pressure and velocity with the convergence condition that the relative residual of pressure equation is less than 1.0×10^{-10}, as described in Eq. (19). The solid wall is regarded as a fluid with a velocity of 0, and its temperature field is solved together with the fluid with the convergence condition of $err < 1.0 \times 10^{-6}$. All discrete equations are solved by the algebraic multigrid method, and the OpenMP parallel algorithm is adopted to improve the solving efficiency,

$$err = \frac{\|\boldsymbol{Ax} - \boldsymbol{b}\|}{\|\boldsymbol{b}\|} \leq 1.0 \times 10^{-10}, \quad (19)$$

where err represents the relative residual; A, x, and b are the coefficient matrix, unknown variable vector, and source term vector of algebraic equations, respectively.

B. Model verification

Numerical simulations of flow-boiling heat transfer are conducted based on uniform and regular hexahedral grids. The height of the solid and fluid grids is inconsistent in the direction perpendicular

to the heating wall, with the former being fixed at $20\,\mu$m. The size of the fluid mesh is determined by a mesh independence test. Two sets of grids with 312 500 and 439 040 fluid nodes are selected to compare the difference in average wall superheat after the flow boiling becomes dynamically stable, corresponding to 15.02 and 14.48 K, respectively, based on a heat flux of $250\,\text{kW/m}^2$. The relative error of the average wall superheating between these two grids is 3.60%, which is acceptable considering the complexity of flow-boiling heat transfer. Therefore, the following simulation work is conducted based on the first grid, with a total of 437 500 nodes, including 312 500 fluid nodes and 125 000 solid nodes.

The reliability of the simulation results is verified by comparing them with those predicted by the Gungor–Winterton correlation,[42] as described in the following equations:

$$q = h_{sp,l}(T_w - T_b) + Sh_{nb}(T_w - T_{sat}), \quad (20)$$

$$h_{nb} = 55P_R^{0.12}(-0.4343 \ln P_R)^{-0.55}M^{-0.5}q^{0.67}, \quad (21)$$

$$S = 1/(1 + 1.15 \times 10^{-6}F^2\text{Re}_l^{1.17}), \quad (22)$$

$$F = 1 + 2.4 \times 10^4\text{Bo}^{1.16}, \quad (23)$$

$$\text{Bo} = \frac{q}{Gh}, \quad (24)$$

where T_b is the temperature of the bulk liquid; h_{nb} is the heat transfer coefficient of the nucleate pool boiling, as calculated by Cooper's equation [Eq. (19) in Ref. 43], $\text{W/(m}^2\,\text{K)}$; S is the suppression factor; F is the Reynolds number factor; P_R is the ratio of relative pressure to critical pressure; M is the molecular mass, kg/kmol; $\text{Bo} = q/Gh$ is the boiling number; and G is the mass flux, kg/m^2 s.

As shown in Fig. 4, the trend in the predicted results obtained by the present numerical simulation is basically consistent with that obtained by the Gungor–Winterton correlation, and the average relative error between the two sets of results is 17.12%. The reasons for the difference mainly include the following three aspects: (i) the length-diameter ratio of the simulated pipe in this study is only 20, which is
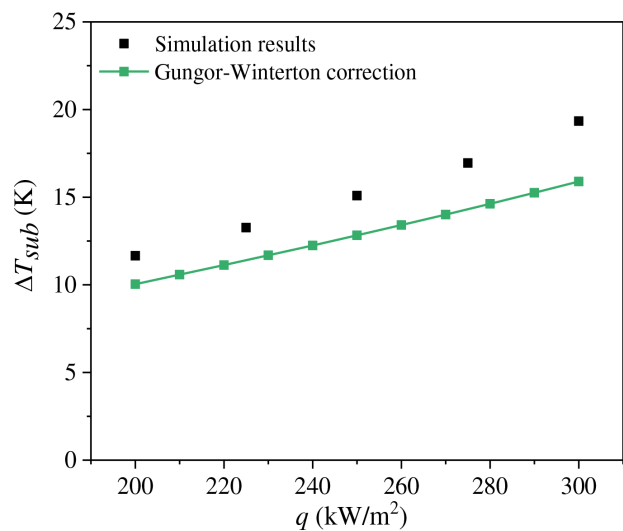

FIG. 4. Comparison of wall superheating predicted by the present numerical simulation method and the Gungor–Winterton correlation.

TABLE II. Physical properties in the experiment.

	Density (kg/m^3)	Viscosity (Pa s)	Thermal conductivity (W/(m K))	Heat capacity (J/(kg K))
Inconel 600	8291	…	14.773	481.04
Liquid	898.65	1.61×10^{-4}	0.6776	4368.3
Vapor	4.013	1.46×10^{-5}	0.034 55	2581.4

less than that of general experimental pipes; (ii) the fluid is only heated by one side of the channel, whereas experiments typically use full perimeter heating; and (iii) the experimental data used in the correlation fitting are mainly based on a circular tube, and most of them are under atmospheric pressure, whereas the research object in this study is a rectangular tube under high pressure.

Furthermore, comparisons in the flow pattern and average wall superheating between simulation and experiment results are made. Next, the experimental conditions are briefly introduced. The tested pipe section is rectangular with a size of 10×10 mm^2, and the length of the visual part is 90 mm. The water with a subcooling of 11.2 K flows into the channel at 99.72 kg/m^2 and exchanges heat with Inconel 600, whose heating power is 0.2136 kW. The system pressure is 0.768 MPa, and the corresponding saturation temperature, latent heat, and surface tension are 441.98 K, 2.05×10^6 J/kg, and 0.044 66 N/m, respectively. Other properties are listed in Table II.

Figure 5 displays the comparison in flow pattern between experiment and simulation in the stable stage. The bubbly flow is obtained by both experiment and simulation methods, and the bubble size is similar. However, compared with the experiment, more bubble number is observed in the simulation, and the mismatch of nucleus site density contributes to this difference. In addition, the average wall
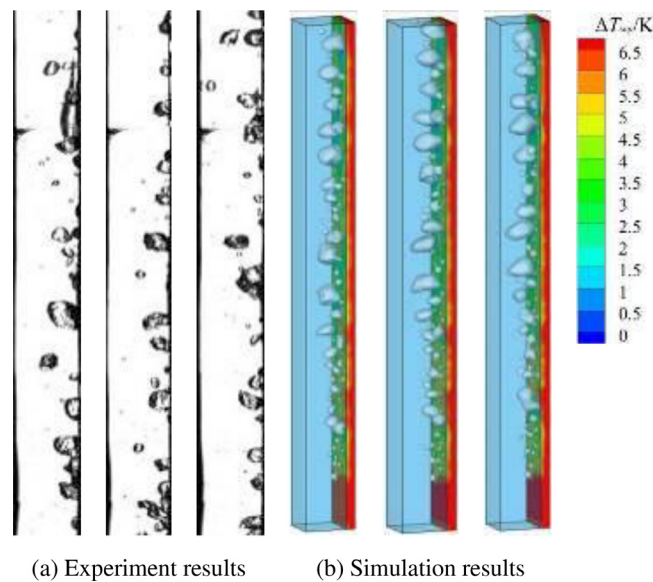

(a) Experiment results   (b) Simulation results

FIG. 5. Comparison in flow pattern between (a) experiment and (b) simulation in the stable stage.

superheat predicted by the simulation method is 6.45 K, which is larger than the 5.10 K obtained by the experiment tool, with a relative difference of 26.37%.

The above comparisons indicate that the predicted deviation of the present simulation is within 30%, which is acceptable for the simulation study of flow-boiling heat transfer.

IV. RESULTS AND DISCUSSION

In this section, the differences in the flow pattern and heat exchange of subcooled flow boiling in an inclined rectangular mini-channel are highlighted and discussed. The reasons for these differences are illustrated through quantitative comparisons revealing the effects of the inclination angle on flow boiling under a low flow rate.

A. Qualitative analyses of flow patterns and wall superheating distributions

Flow-boiling heat transfer is directly related to the flow pattern. First, the similarities and differences in the flow patterns and wall superheating distributions of subcooled flow boiling under different inclination conditions are introduced. In Fig. 6, light blue and transparent white represent the liquid and liquid–vapor interface, respectively, and the wall color is related to the wall superheating ($\Delta T_{sup}=T_w-T_{sat}$). For convenience, all simulation results in Fig. 6 are displayed in a horizontal channel, and the inclination angle is given in the figure subtitle. Differently, Fig. 7 (Multimedia view) shows the videos of subcooled flow boiling in inclined mini-channels, which are displayed in a vertical channel. When a constant heat flux of 300 kW/m^2 is added to the outside of the wall, the wall temperature increases with time, and some nuclei are activated to form different flow patterns and wall superheating distributions.

The flow pattern remains almost the same in the mini-channel as the inclination angle increases from 0° to 180°. When the heating time is less than 100 ms, only a few bubbles have been activated, and the flow pattern is a small bubbly flow. As time goes on, more bubbles are activated. These bubbles grow and coalesce with each other to generate big bubbles with the forward flow. As a result, a small bubbly flow appears in the first half of the mini-channel, which transitions to a large bubbly flow in the second half of the mini-channel over 200 ms. Finally, the flow pattern reaches dynamic stability after 250 ms. Some elongated bubbles can be observed near the outlet, but a stable slug flow is not formed.

The typical single bubble behaviors and dynamics are also similar in different inclined mini-channels. The present macro method cannot reasonably describe the bubble nucleation, and only the detachment, slippage, coalescence, shrinkage, and growth of bubbles are analyzed next based on the horizontal mini-channel. As shown in Fig. 8, two bubbles marked by blue and red arrows are taken as representative ones, which adhere to the heating wall at 70 ms. After 5 ms, the second bubble (red arrow) detaches from the heating wall due to the chaotic flow field and external forces, while the first bubble (blue arrow) keeps slipping along the flow direction. The first slipping bubble gradually grows because of the evaporation at the three-phase contact line and coalescence with around small-sized bubbles, as shown in Figs. 8(f) and 8(g). As heating time increases, the first bubble converts into an elongated one at 190 ms, as described in Fig. 8(i). Differently, once the second bubble gets into the subcooled liquid, the shrinkage phenomenon happens, and its volume decrease with increasing time after 80 ms, as displayed in
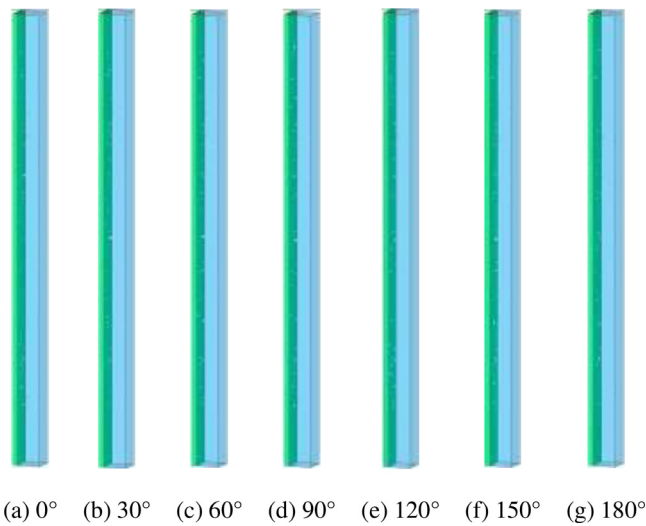
FIG. 6. Representative snapshots of subcooled flow boiling in inclined mini-channels at (a) 0°, (b) 30°, (c) 60°, (d) 90°, (e) 120°, (f) 150°, and (g) 180°.

FIG. 6. (*Continued.*)

Figs. 8(c)–8(g). Finally, the second bubble is artificially removed when it is totally inside one grid because of the failure of the interface reconstruction method. In addition, the forward speed of the second bubble is larger than the first one because of the difference in viscous effect. These two types of bubble behavior induce the formation and evolution of different flow patterns in the studied mini-channel.

A careful comparison suggests that the bubble distribution varies with the inclination angle. At the initial stage (∼100 ms), as shown in Figs. 6(a) and 6(b), when the inclination angle is small, a large number of bubbles detach from the heating wall under the effect of gravity. With an increase in the inclination angle, the gravitational effect on bubble detachment weakens or becomes counterproductive. As shown in Figs. 6(c)–6(g), the number of small bubbles detaching from the heating wall decreases as the inclination angle increases, and more bubbles tend to slip on the wall along the flow direction.

Over time, more small bubbles coalesce in the middle and downstream of the mini-channel to form large bubbles. Almost all of these big bubbles slip on the heating wall under all inclination angles,

(a) 0°   (b) 30°   (c) 60°   (d) 90°   (e) 120°   (f) 150°   (g) 180°

FIG. 7. Videos of subcooled flow boiling in inclined mini-channels at (a) 0°, (b) 30°, (c) 60°, (d) 90°, (e) 120°, (f) 150°, and (g) 180°. Multimedia views: https://doi.org/10.1063/5.0115599.1; https://doi.org/10.1063/5.0115599.2; https://doi.org/10.1063/5.0115599.3; https://doi.org/10.1063/5.0115599.4; https://doi.org/10.1063/5.0115599.5; https://doi.org/10.1063/5.0115599.6; https://doi.org/10.1063/5.0115599.7

indicating that the bubble behavior is independent of the inclination angle. Furthermore, the adjacent large bubbles may merge into slightly elongated bubbles under the limitation of the channel size, but elongated bubbles do not always appear in the mini-channel during the dynamic stable stage. Figure 9 shows that inclination angles of 90° and 180° have a slightly lower probability of forming elongated bubbles, which is obtained by identifying a sequence of flow pattern snapshots.
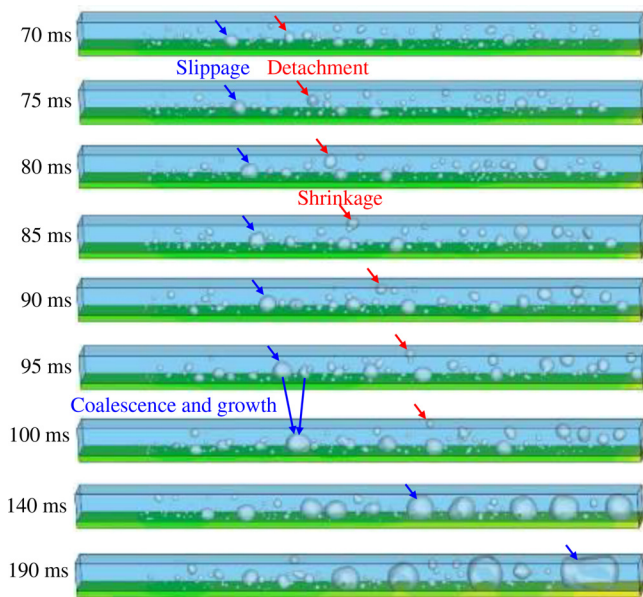

FIG. 8. Representative snapshots of single bubble behavior and dynamics in the horizontal mini-channel.
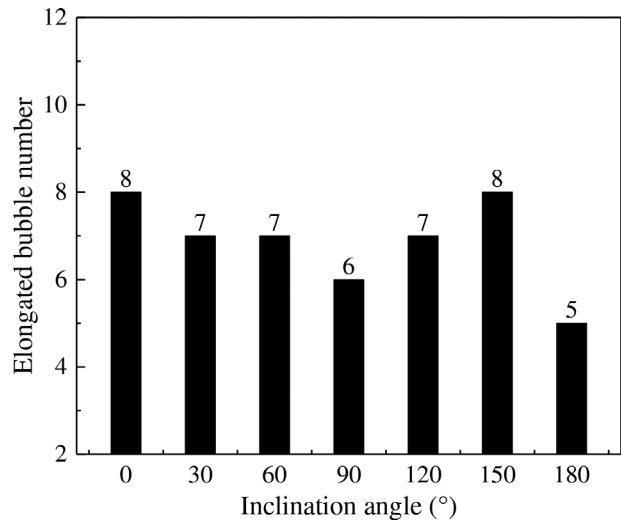
FIG. 9. Elongated bubble numbers at different inclination angles of the mini-channel after 250 ms.

The acting force on the large bubbles in the mini-channel is now qualitatively analyzed to explain why the inclination angle has little effect on the flow pattern. During flow boiling, as shown in Fig. 10(a), the bubbles in a traditional channel mainly suffer surface tension force (F_s), buoyancy force (F_g), unsteady drag force (F_{du}), quasi-steady drag force (F_{qs}), shear lift force (F_{sL}), contact pressure force due to bubble being in contact with the wall (F_{cp}), and hydrodynamic pressure force (F_h).[3,4] The asymmetrical growth of the bubble contributes to the unsteady drag force. In the mini-channel, there is an additional important component of the unsteady drag force acting on the bubble: the impact force. As shown in Fig. 10(b), the liquid flow area is greatly compressed in the mini-channel when large bubbles are present. The liquid flows faster than the big bubble because the latter suffers the viscous effect and surface tension force. Therefore, the liquid velocity in
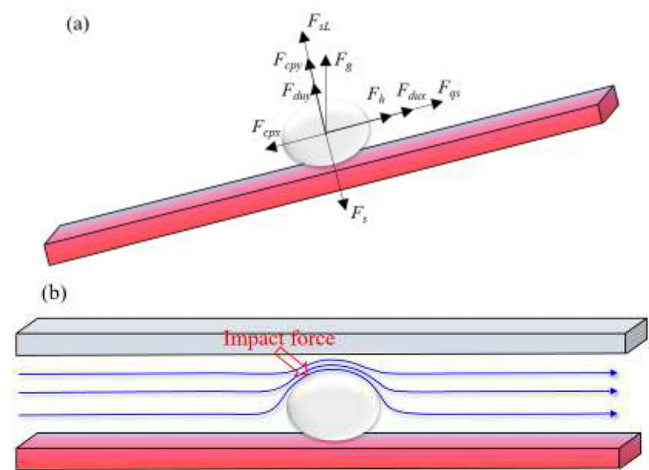
FIG. 10. Sketch of forces on a single bubble in the mini-channel: (a) main force and (b) impact force.

the same cross section as a big bubble will increase, and an upward component of liquid velocity is brought into being due to the impact force from this big bubble based on the momentum theorem. Simultaneously, an opposite impact force toward the heating wall is on the big bubble, resulting in the big bubble sticking to the wall surface and slipping downstream. Additionally, bubbles forming on the heating wall tend to gather nearby to form large bubbles. Under the effect of the liquid flow, these big bubbles easily remain in contact with the heating wall or coalesce with other bubbles that have not detached from the heating wall, as marked in Fig. 11, encouraging them to slip along the heating wall regardless of the inclination angle. In short, although the flow rate is very low, big bubbly flow occurs independently of the inclination angle, with large bubbles sliding along the flow direction on the middle and downstream heating wall of the mini-channel once the flow boiling has become stable.

During the dynamically stable stage, a small bubbly flow appears upstream of the rectangular mini-channel at various inclination angles. The generation and movement of these small bubbles break the temperature boundary layer, keeping the temperature at a low level with a relatively uniform distribution under different inclination conditions. However, the larger bubbles downstream tend to slip on the heating wall, forming a distinct dry patch below, resulting in a slight deterioration in the local heat exchange and the formation of a high-superheating region. Under the sliding of large bubbles, these local dry patches can be rewetted and re-cooled by liquid. However, once the elongated bubbles appear, the dry patch area becomes larger and requires longer to be rewetted, leading to the formation of hotspots, as depicted by the darker red color of the wall in Fig. 6. Under the effect of wall heat conduction and the periodic wetting of dry patches, the local wall superheating rises and falls periodically without triggering the boiling crisis in the second half of the mini-channel at 300 kW/m². Qualitatively, there is no obvious difference in the superheating distribution at different inclination angles. More detailed quantitative analyses of heat transfer will be presented in Sec. IV B.

In summary, under a low mass flow rate, the existence of a liquid impact force different from the macro-channel case causes that the flow pattern in the mini-channel changing little with respect to the inclination angle, and larger bubbles in the middle and downstream reaches tend to slip on the heating wall along the flow direction. The dry patches are rewetted with the slipping of large/elongated bubbles periodically, leading to a periodic change in the local wall superheating in the second half of the mini-channel, without noticeable difference under different inclination angles.

B. Quantitative analyses of flow-boiling heat transfer

The quantitative similarities and differences in the average, local, and maximum wall superheating under different inclination angles are discussed in this subsection. For illustration convenience, some superheating-related variables are defined as follows: ΔT_{sup} represents the spatial average superheating of the whole wall surface; $\Delta T_{sup,\ ave}$ and $\Delta T_{sup,\ loc}$ express the temporal-spatial average superheating of the

whole and local wall surface in the dynamically stable stage; and $\Delta T_{sup,\ max}$ is the maximum local superheating of wall surface.

Figure 12 shows the profiles of the average wall superheating (ΔT_{sup}) with time under different inclination angles. The average wall superheating can be divided into three stages: the first stage is from 0 to 0.05 s, where the wall superheating under different inclination angles almost coincides; the second stage is from 0.05–0.25 s, where the wall superheating begins to differ with inclination angle, and the difference increases with the heating time; the third stage is after 0.25 s, at which time the wall superheating under different inclination angles remains dynamically stable. As shown in Fig. 13, in the stable stage, there is a slight difference in the spatiotemporal average wall superheating of mini-channels with inclination angles of 0°–90°, for which the wall superheating is slightly lower than in mini-channels with inclination angles of 120°–180°. However, the maximum relative difference is only 8.4% among the different inclination angles.

The flow boiling is stable in the third stage. Although the flow patterns (small bubbly flow in the middle and upper reaches, large bubbly flow in the lower reaches) and average heat exchange performance at different inclination angles are almost the same, the inclination angle has some impact on the local boiling heat transfer characteristics. The local HTC is calculated by Eq. (25). Figures 14 and 15 illustrate the profiles of local wall superheating and the local HTC along the flow direction under different inclination angles during the dynamically stable stage. In the middle and upper reaches of the mini-channel, the heat exchange intensity gradually increases along the flow direction, but it varies greatly under different inclination angles. The heat exchange intensity is high for inclination angles near 0°, and the corresponding wall superheating is lower. In contrast, as the inclination angle approaches 180°, the heat transfer intensity becomes lower and the wall superheating increases. In the downstream reaches of the mini-channel, the heat exchange intensity gradually decreases along the flow direction, and the wall superheating begins to rise rapidly with the formation of dry patches. Similarly, the rate of increase is distinct under different inclination angles: (i) the heat transfer
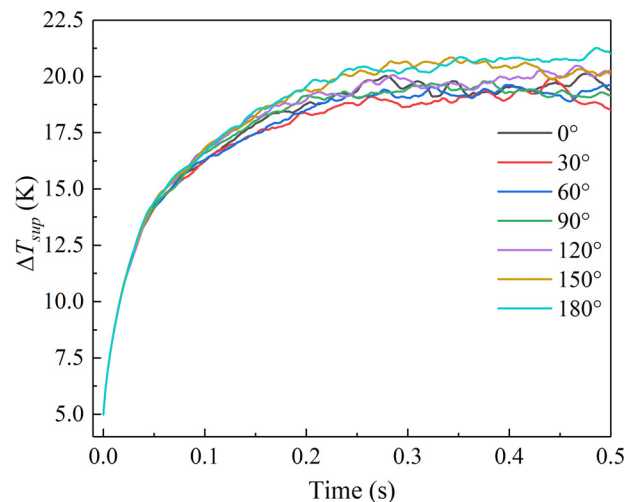

FIG. 11. Sketch of bubble coalescence.

FIG. 12. Profiles of average wall superheating with time under different inclination angles.

FIG. 13. Average wall superheating under different inclination angles during the dynamically stable stage.
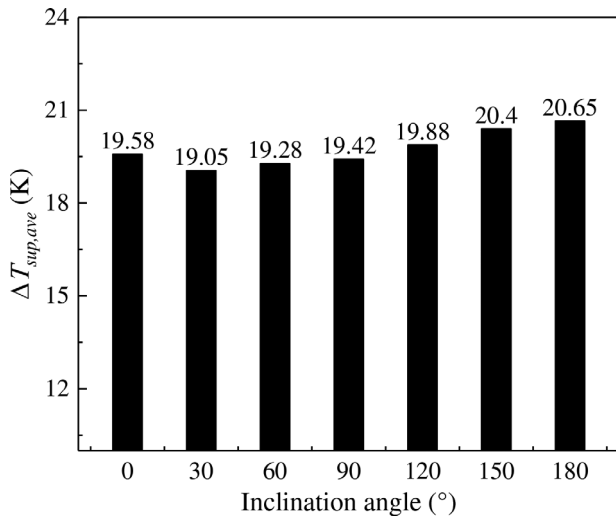

FIG. 15. Profile of HTC under different inclination angles during the dynamically stable stage.

deteriorates significantly when the inclination angle is near 0°, and the wall superheating increases rapidly; (ii) when the mini-channel has an inclination angle close to 90°, the heat exchange intensity is relatively high, the rate of increase in wall superheating is relatively slow, and the superheating at the outlet is the lowest of all the inclination angles; and (iii) the heat transfer intensity of the mini-channel is still low as the inclination angle is close to 180°, but the wall superheating does not exhibit a rapid increment,

$$\mathrm{HTC}_{loc} = \sum_{t_0=250ms}^{t_1=500ms} \frac{q_{w,loc}}{\left(T_{w,loc} - T_{b,loc}\right)} \Big/ (t_1 - t_0), \qquad (25)$$

where $q_{w,loc}$ is the heat flux of the local wall surface obtained by the transient wall heat conduction, W/m²; $T_{w,loc}$ is the temperature of the local wall surface, K; $T_{b,loc}$ is the temperature of local bulk fluid, K.
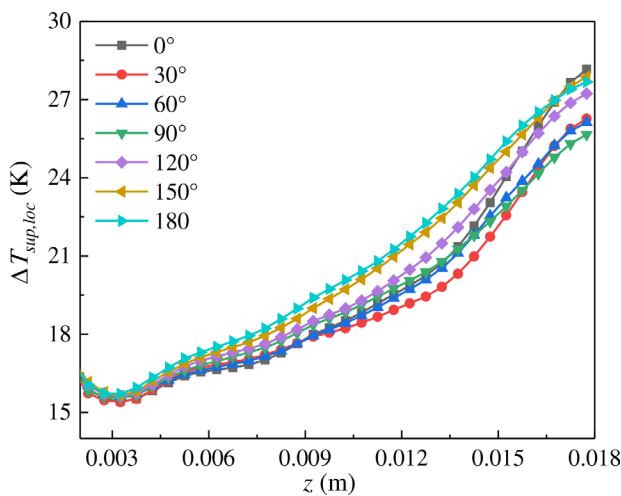

FIG. 14. Profile of local wall superheating under different inclination angles during the dynamically stable stage.
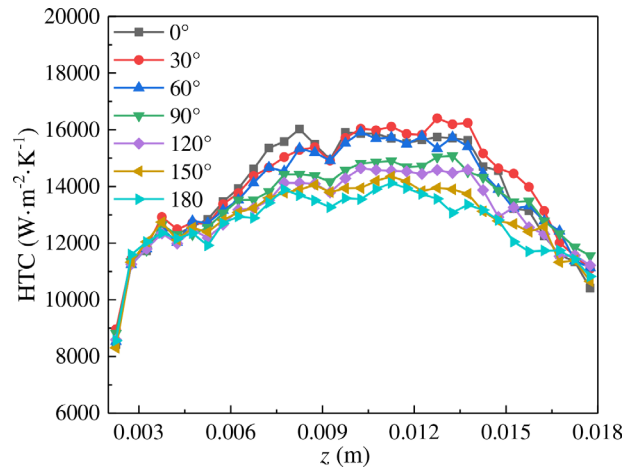
The reasons for the similarities and differences of the above-mentioned three stages of boiling heat transfer under different inclination angles are now analyzed. In the first stage (0–50 ms), the typical small bubbly flow pattern is illustrated in Fig. 6 at 20 and 50 ms. Compared with forced convection, gravity has little effect on the movement of these small bubbles, and the single-phase convection is strong during this stage. Therefore, the heat exchange intensity between the fluid and the wall under different inclination angles is equivalent, resulting in a slight difference in the wall superheating. In the second stage (50–250 ms), as shown in Fig. 6, numerous small bubbles gather and merge into medium-size bubbles at 100 ms. Gravity begins to affect these bubbles, and they tend to detach from the wall when the inclination angle is near 0°, leading to lower wall superheating. In contrast, gravity prevents the bubbles from leaving the heating wall at inclination angles close to 180°, causing higher wall superheating. Furthermore, the bubble volume expands with the heating time, and the role of gravity becomes more prominent. Hence, the difference in average wall superheating among different inclination angles increases.

In the third stage (>250 ms), the flow boiling is dynamically stable. The heat transfer characteristics of flow boiling in the inclined mini-channels are mainly affected by two factors: the detachment of medium/small bubbles in the middle and upper reaches and the slipping velocity of large/elongated bubbles in the downstream reaches. In the middle and upper reaches of the mini-channel, the gravity effect favors the detachment of medium/small-sized bubbles in the mini-channel near 0°, so the wall superheating is relatively low, as shown in Fig. 14. In the downstream reaches of the mini-channel, the effect of gravity on the detachment of larger bubbles can be ignored because of the impact force. For inclination angles close to 90°, gravity encourages large/elongated bubbles to slip away from the mini-channel rapidly so that the dry patches below are rewetted more quickly, leading to lower wall superheating near the outlet, as shown in Fig. 14. However, for mini-channels with inclination angles near 0° or 180°, the bubble slip speed is slower, which is less conducive to the rewetting of dry patches. This results in higher wall superheating near the outlet. To further highlight the effect of gravity on the sliding velocity of

larger bubbles, inclination angles of 0° and 90° are selected to track representative bubbles of similar sizes, and their moving distances are calculated within the same time period. As shown in Fig. 16, from 200 to 225 ms, the moving distance of the target bubble in the mini-channel with an inclination angle of 0° is about 2.1 mm (0.084 m/s), whereas that for the inclination angle of 90° is about 3.0 mm (0.12 m/s). The latter is about 1.43 times the former. Therefore, the slipping speed of the large bubble is faster for the mini-channel inclined at 90°, destroying the temperature boundary layer and rewetting the dry patch quickly. As shown in Fig. 17, it is not easy to form local high superheating at an inclination angle of 90°. Based on the above analyses of heat exchange in the third stage, it can be concluded that gravity has positive effects on reducing wall superheating for channels with inclination angles of 0°–90°. For inclination angles of 90°–180°, gravity has both positive and negative effects on heat exchange, and they decrease and increase with the rising of inclination angle, respectively. Therefore, the difference in the average wall superheating among mini-channels inclined at 0°–90° is small, and such channels have an average wall superheating lower than that of mini-channels inclined at 120°–180°.

Some additional heat transfer characteristics of channels inclined at particular angles are now addressed and explained. For mini-channels with inclination angles of 30° and 60°, gravity encourages the bubbles to detach from the heating wall in the middle and upper reaches and accelerates the rewetting of the dry patches in the downstream reaches, leading to the best heat exchange performance (see Figs. 14, 15, and 17). For the mini-channels inclined at 150° and 180°, most bubbles tend to slip on the wall, resulting in higher wall superheating. Simultaneously, the activation of new bubbles is restrained to a certain extent, leading to lower bubble volumes downstream and smaller dry patches. Therefore, the wall superheating grows at a relatively low rate in the downstream reaches of the mini-channel, as shown in Fig. 14. At inclination angles of 150° and 180°, the maximum wall superheating is 34.37 and 32.13 K, respectively, which is less than the value of 37.48 K in the mini-channel with an inclination angle of 0°.

The dry patch causes the local heat transfer deterioration, which expands and may trigger the boiling crisis with the increase in heat flux. Therefore, for the heat fluxes of 350, 400, 450, and 500 kW/m^2, the effect of inclination angle on the flowing boiling crisis (CHF) is illustrated. Figure 18 displays the trends of maximum local wall superheating with
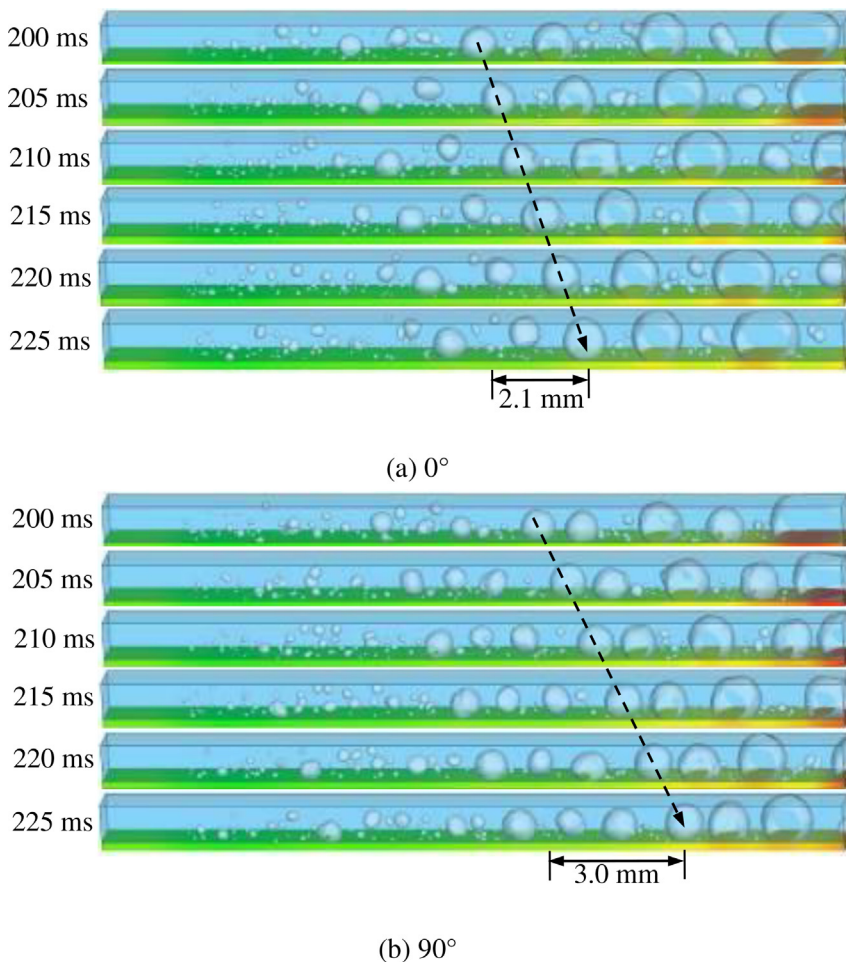

(a) 0°

(b) 90°

FIG. 16. Comparison in moving distance of target bubble between mini-channels inclined at (a) 0°, (b) 90°.
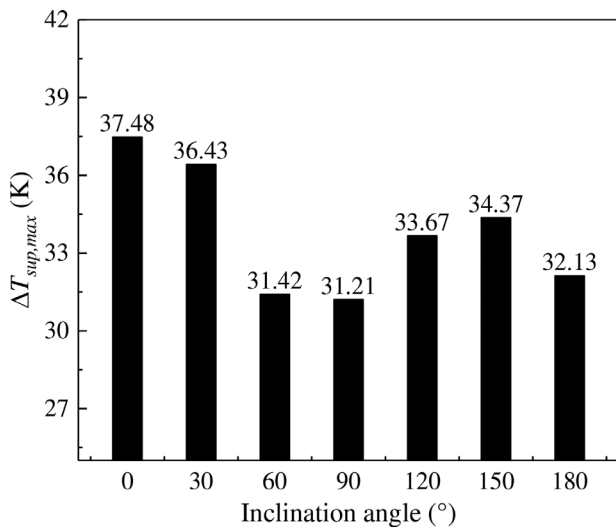
FIG. 17. Maximum local wall superheating in inclined mini-channels.

heat flux in inclined mini-channels at 0°, 90°, and 180° within the simulation time of 500 ms. The maximum local wall superheating increases linearly without sharp change because the dry patch can be rewetted by the pumped liquid. This phenomenon is different from pool boiling that the liquid cannot feed when a vapor film covers the heating surface leading to the soaring of wall superheating. Therefore, in this study, it is hard to obtain CHF directly, which can be determined by wall properties. Next, the maximum local wall superheating in inclined mini-channels is compared. As described in Fig. 18, the inclination effect on maximum local wall superheating becomes indeterminacy under the high heat flux exceeding 350 kW/m². The advantage of the inclined mini-channel at 90° in accelerating bubble slippage and reducing local wall superheating disappears. The reason for that can be explained by the representative
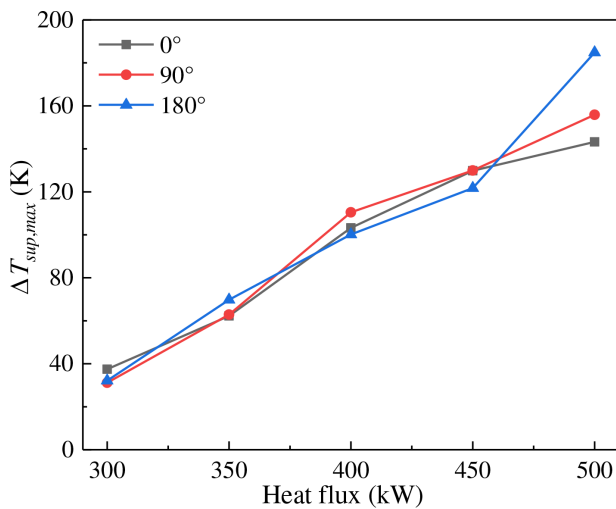

FIG. 18. Trends of maximum local wall superheating with heat flux in inclined mini-channels.

snapshots of subcooled flow boiling when the added heat flux is high. As shown in Fig. 19, under the heat flux of 500 kW/m², the slug flow happens in the middle and down reaches of the inclined mini-channel at 180°. Many elongated bubbles appear and occupy the whole section of the mini-channel, leading to alternating of the liquid segment and vapor slug. As a result, because the liquid is incompressible, the slipping velocity of these elongated bubbles (the rewetting of dry patches below these elongated bubbles) is independent of gravity based on the volume continuity equation. The moving velocity of the elongated bubble is decided by the inlet velocity and bubble volume change induced by phase transition at the vapor-liquid interface. In addition, the required time of rewetting of the local dry patch increases due to the coalescence of two adjacent elongated bubbles, leading to the appearance of a maximum local wall superheating. The elongated bubble coalescence is related to its dynamics but is also independent of gravity. Therefore, there are irregular differences among inclined mini-channels in maximum local wall superheating under high heat fluxes, and the inclination angle does not affect the CHF of flow boiling.

In summary, the maximum relative differences in the average and maximum local wall superheating after the flow boiling becomes stable are 8.4% and less than 22.5%, respectively, across the different inclination angles considered in this study. This indicates that the inclination angle has a very limited effect on flow-boiling heat transfer in rectangular mini-channels under low flow rates. This conclusion is consistent with the experimental results of Chen et al.,[18] which showed that the boiling curves in a mini-channel with a hydraulic diameter of 0.91 mm are almost coincident over inclination angles of −90°–90°. Both the numerical simulation results in this paper and the research in Ref. 18 prove that the inclination angle has no significant effect on the flow-boiling heat transfer in mini-channels at low flow rates, which is different from the case in macro-channels.[9–16,20,21]

V. CONCLUSIONS

This paper has discussed flow boiling in different three-dimensional inclined mini-channels at a low flow rate by a relatively accurate numerical simulation method using the VOSET method and considering the conjugate heat transfer and a reasonable nucleus site density model. The inclination angle was found to have only slight effects on the flow pattern and heat transfer of flow boiling in the mini-channel, and the reasons for that were revealed. The major conclusions are summarized as follows.

(1) When the heat flux is 300 kW/m², the inclination angle only slightly affects the flow pattern of flow boiling in a mini-channel at low flow rates. For inclination angles of 0°–180°, a small bubbly flow occurs upstream of the channel, and this gradually transitions to a large bubbly flow downstream. The flow area shrinks with the growth of the bubbles, leading to the formation of an impact force that causes the larger bubbles to slip on the heating wall under different inclination angles. To our knowledge, this impact force is first addressed in this study, which can be neglected in macro-channels.

(2) The inclination angle has several effects on the local heat transfer characteristics of inclined mini-channels as the heat flux is 300 kW/m². Gravity affects the bubble behavior from two aspects: (i) promoting small/medium bubbles to detach from the heating wall and enhancing heat transfer; (ii) encouraging large/elongated bubbles to leave the channel and strengthening
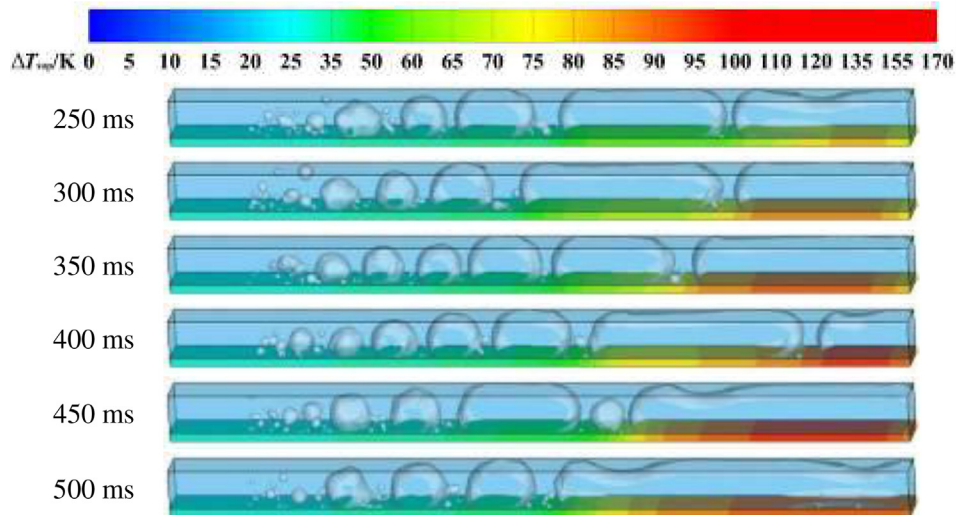
FIG. 19. Representative snapshots of flow boiling in inclined mini-channel at 180°.

the rewetting of dry patches. Therefore, the HTC in the upper and middle reaches is high for the mini-channel inclined at angles close to 0° because of the first effect, and the wall super-heating is lower near the outlet for mini-channels inclined at around 90° under the second effect. Overall, the heat transfer performance of mini-channels inclined at 0°–90° is better, but the biggest benefit is only 8.4% in terms of the average wall superheating.

(3) The maximum local wall superheating becomes lower as the inclination angle approaches 90° when the heat flux is 300 kW/m^2. Because of the impact force, larger bubbles tend to slip along the flow direction on the heating wall, generating dry patches below, which results in a local temperature rise. Gravity has a positive effect on pushing the bubbles away from the mini-channel at angles near 90°, leading to an accelerated rewetting of the dry patches and a lower local maximum wall superheating. However, this positive effect disappears with the increase in heat flux because of the happening of slug flow. Briefly, the maximum relative difference is only 22.5% among the various inclination angles considered here, which is still small from the perspective of the complex heat exchange of flow boiling.

SUPPLEMENTARY MATERIAL

See the supplementary material for describing the bubble nucleation.

ACKNOWLEDGMENTS

AUTHOR DECLARATIONS
Conflict of Interest

The authors have no conflicts to disclose.

Author Contributions

Yujie Chen: Conceptualization (equal); Formal analysis (equal); Investigation (equal); Methodology (equal); Software (equal); Writing – original draft (equal). **Ge-Ge Song:** Investigation (equal); Writing – review & editing (equal). **Kong Ling:** Investigation (equal); Methodology (equal); Software (equal). **Bo Yu:** Conceptualization (equal); Funding acquisition (equal); Supervision (equal). **Dongliang Sun:** Conceptualization (equal); Funding acquisition (equal); Methodology (equal); Resources (equal). **Wei Lu:** Formal analysis (equal); Validation (equal); Visualization (equal). **Wenquan Tao:** Funding acquisition (equal); Methodology (equal); Supervision (equal); Writing – review & editing (equal).

DATA AVAILABILITY

The data that support the findings of this study are available from the corresponding author upon reasonable request.

REFERENCES

[1] L. Cheng and G. Xia, "Fundamental issues, mechanisms and models of flow boiling heat transfer in microscale channels," Int. J. Heat Mass Transfer **108**, 97 (2017).
[2] X. Fang, Y. Yuan, A. Xu, L. Tian, and Q. Wu, "Review of correlations for sub-cooled flow boiling heat transfer and assessment of their applicability to water," Fusion Eng. Des. **122**, 52 (2017).
[3] R. Situ, T. Hibiki, M. Ishii, and M. Mori, "Bubble lift-off size in forced convective subcooled boiling flow," Int. J. Heat Mass Transfer **48**, 5536 (2005).
[4] G. H. Yeoh and J. Y. Tu, "A unified model considering force balances for departing vapour bubbles and population balance in subcooled boiling flow," Nucl. Eng. Des. **235**, 1251 (2005).

[5]J. Wang, W. Guo, K. Xiong, and S. Wang, "Review of aerospace-oriented spray cooling technology," Prog. Aerosp. Sci. **116**, 100635 (2020).

[6]A. Dhruv, E. Balaras, A. Riaz, and J. Kim, "An investigation of the gravity effects on pool boiling heat transfer via high-fidelity simulations," Int. J. Heat Mass Transfer **180**, 121826 (2021).

[7]V. Kishor, S. Singh, and A. Srivastava, "Flow instabilities and heat transfer in a differentially heated cavity placed at varying inclination angles: Non-intrusive measurements," Phys. Fluids **33**, 094103 (2021).

[8]C. Konishi and I. Mudawar, "Review of flow boiling and critical heat flux in microgravity," Int. J. Heat Mass Transfer **80**, 469 (2015).

[9]H. Zhang, I. Mudawar, and M. M. Hasan, "Experimental and theoretical study of orientation effects on flow boiling CHF," Int. J. Heat Mass Transfer **45**, 4463 (2002).

[10]C. R. Kharangate, L. E. O'Neill, and I. Mudawar, "Effects of two-phase inlet quality, mass velocity, flow orientation, and heating perimeter on flow boiling in a rectangular channel. II. CHF experimental results and model," Int. J. Heat Mass Transfer **103**, 1280 (2016).

[11]C. O. Gersey and I. Mudawar, "Effects of orientation on critical heat flux from chip arrays during flow boiling," J. Electron. Packag. **114**, 290 (1992).

[12]H. Zhang, I. Mudawar, and M. M. Hasan, "Experimental assessment of the effects of body force, surface tension force, and inertia on flow boiling CHF," Int. J. Heat Mass Transfer **45**, 4079 (2002).

[13]H. Zhang, I. Mudawar, and M. M. Hasan, "A method for assessing the importance of body force on flow boiling CHF," ASME J. Heat Transfer **126**, 161 (2004).

[14]M. Piasecka and B. Maciejewska, "The study of boiling heat transfer in vertically and horizontally oriented rectangular minichannels and the solution to the inverse heat transfer problem with the use of the Beck method and Trefftz functions," Exp. Therm. Fluid Sci. **38**, 19 (2012).

[15]M. Piasecka, "Correlations for flow boiling heat transfer in minichannels with various orientations," Int. J. Heat Mass Transfer **81**, 114 (2015).

[16]M. Piasecka and B. Maciejewska, "Heat transfer coefficient during flow boiling in a minichannel at variable spatial orientation," Exp. Therm. Fluid Sci. **68**, 459 (2015).

[17]J. Hu, C. Sun, X. Xu, and X. Liang, "The experiments of inclination effect on flow boiling heat transfer," J. Eng. Thermophys. **32**, 101 (2011).

[18]B. Chen, L. Dong, X. Tao, J. Wang, X. Zhao, and J. Cao, "Investigation on gravity independence of flow boiling heat transfer in parallel micro/mini-channels," Aerosp. Shanghai **3**, 118 (2016).

[19]Y. Mei, "Study on two-phase flow and critical heat flux mechanism in an inclined rectangular channel under low flow rates," Ph.D. thesis (Shanghai Jiaotong University, 2018).

[20]Y. Mei, Y. Shao, S. Gong, Y. Zhu, and H. Gu, "Effects of surface orientation and heater material on heat transfer coefficient and critical heat flux of nucleate boiling," Int. J. Heat Mass Transfer **121**, 632 (2018).

[21]G. B. Abadi, C. Moon, and K. C. Kim, "Effect of gravity vector on flow boiling heat transfer, flow pattern map, and pressure drop of R245fa refrigerant in mini tubes," Int. J. Multiphase Flow **83**, 202 (2016).

[22]S. S. Mehendafe, A. M. Jacobi, and R. K. Shah, "Fluid flow and heat transfer at micro- and meso-scales with application to heat exchanger design," Am. Soc. Mech. Eng. **53**, 175 (2000).

[23]I. Yeo and S. Lee, "2D computational investigation into transport phenomena of subcooled and saturated flow boiling in large length to diameter ratio microchannel heat sinks," Int. J. Heat Mass Transfer **183**, 122128 (2022).

[24]D. Lorenzini and Y. Joshi, "Flow boiling heat transfer in silicon microgaps with multiple hotspots and variable pin fin clustering," Phys. Fluids **31**, 102002 (2019).

[25]D. Nie and G. Guan, "Study on boiling heat transfer in a shear flow through the lattice Boltzmann method," Phys. Fluids **33**, 043314 (2021).

[26]Y. Yu, Q. Li, Y. Qiu, and R. Z. Huang, "Bubble dynamics and dry spot formation during boiling on a hierarchical structured surface: A lattice Boltzmann study," Phys. Fluids **33**, 083306 (2021).

[27]L. Chen, Q. Kang, Y. Mu, Y. He, and W. Tao, "A critical review of the pseudo-potential multiphase lattice Boltzmann model: Methods and applications," Int. J. Heat Mass Transfer **76**, 210 (2014).

[28]Q. Li, K. H. Luo, Q. J. Kang, Y. L. He, Q. Chen, and Q. Liu, "Lattice Boltzmann methods for multiphase flow and phase-change heat transfer," Prog. Energy Combust. Sci. **52**, 62 (2016).

[29]D. Li and V. K. Dhir, "Numerical study of single bubble dynamics during flow boiling," ASME J. Heat Transfer **129**, 864 (2007).

[30]R. Chen, W. Tian, G. H. Su, S. Qiu, Y. Ishiwatari, and Y. Oka, "Numerical investigation on bubble dynamics during flow boiling using moving particle semi-implicit method," Nucl. Eng. Des. **240**, 3830 (2010).

[31]M. Vermaak, J. Potgieter, J. Dirker, M. A. Moghimi, P. Valluri, K. Sefiane, and J. P. Meyer, "Experimental and numerical investigation of micro/mini channel flow-boiling heat transfer with non-uniform circumferential heat fluxes at different rotational orientations," Int. J. Heat Mass Transfer **158**, 119948 (2020).

[32]Y. Zhang, Q. Hao, and B. Geng, "Numerical simulation on flow boiling of R32 in inclined microchannel," Cryog. Supercond. **48**, 62 (2020).

[33]F. Gibou, L. Chen, D. Nguyen, and S. Banerjee, "A level set based sharp interface method for the multiphase incompressible Navier–Stokes equations with phase change," J. Comput. Phys. **222**, 536 (2007).

[34]C. R. Kharangate and I. Mudawar, "Review of computational studies on boiling and condensation," Int. J. Heat Mass Transfer **108**, 1164 (2017).

[35]D. Sun and W. Q. Tao, "A coupled volume-of-fluid and level set (VOSET) method for computing incompressible two-phase flows," Int. J. Heat Mass Transfer **53**, 645 (2010).

[36]K. Ling, Z. Li, D. Sun, Y. He, and W. Tao, "A three-dimensional volume of fluid and level set (VOSET) method for incompressible two-phase flow," Comput. Fluids **118**, 293 (2015).

[37]J. Smagorinsky, "General circulation experiments with the primitive equations," Mon. Weather Rev. **91**, 99 (1963).

[38]M. M. Francois, S. J. Cummins, E. D. Dendy, D. B. Kothe, J. M. Sicilian, and M. W. Williams, "A balanced-force algorithm for continuous and sharp interfacial surface tension models within a volume tracking framework," J. Comput. Phys. **213**, 141 (2006).

[39]Q. Li, Y. Jiao, M. Avramova, P. Chen, J. Yu, J. Chen, and J. Hou, "Development, verification and application of a new model for active nucleation site density in boiling systems," Nucl. Eng. Des. **328**, 1 (2018).

[40]Y. Chen, K. Ling, H. Ding, Y. Wang, S. Jin, and W. Tao, "3-D numerical study of subcooled flow boiling in a horizontal rectangular mini-channel by VOSET," Int. J. Heat Mass Transfer **183**, 122218 (2022).

[41]K. Ling, G. Son, D. Sun, and W. Tao, "Three dimensional numerical simulation on bubble growth and merger in microchannel boiling flow," Int. J. Therm. Sci. **98**, 135 (2015).

[42]K. E. Gungor and R. H. S. Winterton, "A general correlation for flow boiling in tubes and annuli," Int. J. Heat Mass Transfer **29**, 351 (1986).

[43]M. G. Cooper, "Heat flow rates in saturated nucleate pool boiling-a wide-ranging examination using reduced properties," Adv. Heat Transfer **16**, 157 (1984).